International Journal of Chemical, Materials and Biomolecular Sciences
ISSN: 2415-6620
Vol:10, No:6, 2016

Complex Flow Simulation Using a Partially Lagging One-Equation Turbulence Model

M. Elkhoury

***Abstract*—**A recently developed one-equation turbulence model has been successfully applied to simulate turbulent flows with various complexities. The model, which is based on the transformation of the k-ε closure, is wall-distance free and equipped with lagging destruction/dissipation terms. Test cases included shock-boundary-layer interaction flows over the NACA 0012 airfoil, an axisymmetric bump, and the ONERA M6 wing. The capability of the model to operate in a Scale Resolved Simulation (SRS) mode is demonstrated through the simulation of a massive flow separation over a circular cylinder at Re= 1.2 x10^6. An assessment of the results against available experiments Menter $(k\text{-}\varepsilon)_{1Eq}$ and the Spalart-Allmaras model that belongs to the single equation closure family is made.

***Keywords*—**Turbulence modeling, complex flow simulation, scale adaptive simulation, one-equation turbulence model.

I. Introduction

TURBULENCE models are still the choice in almost all engineering applications due to their simplicity, low computational cost, and acceptable accuracy. The latter is an issue of concern to many Computational Fluid Dynamics (CFD) users in the engineering society. Surely, in lieu of utilizing these models, Large Eddy Simulation (LES) can accurately predict complex flows with massive separation, vortex shedding, and strong adverse pressure gradient. However, LES requires larger integration time compared to Unsteady Reynolds Average Navier-Stokes (URANS), smaller time-step, and higher mesh resolution. When combining all these effects with a real-life engineering application, it becomes evident that this approach is prohibitive and users generally revert back to URANS for prompt results, not to mention the advancements that have been made to improve the accuracy of turbulence models.

A one-equation model [1] is constructed following Menter and Egorov [2] SRS concept that is based on the inclusion of the von Karman length scale in their two-equation turbulence k-ω-SST closure. This in turn enables the model to adjust to resolved turbulent structures rather than dissipating them as RANS models do, an ability of the model referred to by Scale-Adaptive Simulation (SAS). These models perform best in globally unstable flows that are associated with massive flow separation, in which they are capable of resolving large- and small-scale turbulent structures. SAS models revert back to RANS mode when insufficient spatial and temporal resolution is encountered.

The main objective of this work is to demonstrate that a simple one-equation turbulence model can accurately simulate challenging engineering problems. The transformation methodology of this partially lagging one-equation model was proposed by Menter [3] using Bradshaw et al. [4], i.e., a constant turbulent structure parameter $\left|-\overline{uv}\right|/k$. The model operates in SRS mode and thus can resolve turbulent scales in flows with massive separation. The SRS concept has been introduced by Menter et. al. who used the $(k\text{-}\varepsilon)_{1Eq}$ one-equation model [5], which was originally derived from the k-ε closure [3]. Following this methodology, Elkhoury [6]-[8] developed several versions of these models, all of which included a second derivative of velocity and thus, operate in SRS mode.

In the present work a partially lagging one-equation turbulence model is applied to challenging turbulent test cases and assessed against other models that belong to the one-equation family closure. Five external aerodynamic flow test cases, two of which are three-dimensional, are used to assess the models' performance.

II. Turbulence Models

The three considered turbulence models are the one-equation SAS model, Menter One-equation model, and the SA model.

A. The SA Turbulence Model

The SA turbulence model [9] was developed and calibrated based on physical arguments in boundary layers and free-shear flows. The model has gained special interest in external aerodynamics and is considered among the mature and well verified models. Excluding the transition term, the SA model can be written as

$$\frac{D\tilde{\nu}_T}{Dt} = c_{b1}\tilde{\Omega}\tilde{\nu}_T + \frac{\partial}{\partial x_j}\left(\frac{(\tilde{\nu}_T+\tilde{\nu})}{\sigma}\frac{\partial\tilde{\nu}_T}{\partial x_j}\right) + c_{b2}\left(\frac{\partial\tilde{\nu}_T}{\partial x_j}\right)^2 - c_{w1}f_w\left(\frac{\tilde{\nu}_T}{d}\right)^2 \quad (1)$$

The modified magnitude of vorticity is given by

$$\tilde{\Omega} = \Omega + \frac{\tilde{\nu}_T}{\kappa^2 d^2}f_{v2} \quad (2)$$

The closure coefficients and damping functions are as:

$$g = r + c_{w2}(r^6 - r),$$

M. Elkhoury is Associate professor of mechanical engineering, Lebanese American University, Byblos-Lebanon (e-mail: mkhoury@lau.edu.lb).

$$c_{w1} = \frac{c_{b1}}{\kappa^2} + \frac{(1+c_{b2})}{\sigma} \quad (3)$$

$$f_{v2} = 1 - \frac{\chi}{1+\chi f_{v1}},\ \chi = \frac{\tilde{\nu}_T}{\nu},\ f_{v1} = \frac{\chi^3}{c_{v1}^3 + \chi^3} \quad (4)$$

$$f_w = g\left[\frac{1+c_{w3}^6}{g^6 + c_{w3}^6}\right]^{1/6},\ r = \frac{\tilde{\nu}_T}{\tilde{\Omega}\kappa^2 d^2} \quad (5)$$

$$c_{b1} = 0.1355,\ c_{b2} = 0.622,\ c_{v1} = 7.1,\ \sigma = 2/3,\ c_{w1} = 0.3, \quad (6)$$

and the damped eddy viscosity is given by

$$\nu_T = \tilde{\nu}_T f_{v1} \quad (7)$$

B. Menter One-Equation (k-ε)1E Turbulence Model

Menter [5] has transformed the *k-ε* closure into a one-equation model herein referred to as Menter (*k-ε*)1E based model using Bradshaw's turbulent structure parameter. The final forms of the original one-equation models may be written as

$$\frac{D\tilde{\nu}_T}{Dt} = C_1 D_1 \tilde{\nu}_T S + \frac{\partial}{\partial x_j}\left(\frac{\tilde{\nu}_T}{\sigma}\frac{\partial \tilde{\nu}_T}{\partial x_j}\right) - C_2 \frac{\tilde{\nu}_T^{\,2}}{L_{VK-SAS}^2} \quad (8)$$

The constants C_2 and C_1 corresponding are calculated based on the values of the standard *k-ε* closure $C_{\varepsilon 1} = 1.44$ and $C_{\varepsilon 2} = 1.92$, with $C_2 = 1.856$ and C_1 follows from the log law, i.e., $C_1 = \kappa^2 (C_2 - 1.0/\sigma)$. The diffusion coefficient was taken based on that of the k-equation, i.e., $\sigma = 1.0$, and the damping function in front of the production term given by

$$D_1 = \frac{\nu_T + \nu}{\tilde{\nu}_T + \nu} \quad (9)$$

The formulation of the inverse of the von Karman mixing length-scale follows as

$$\frac{1}{L_{vK-SAS}^2} = \frac{\left|\frac{\partial^2 U_i}{\partial x_j^2}\frac{\partial^2 U_i}{\partial x_k^2}\right|}{\left|\frac{\partial U_i}{\partial x_j}\frac{\partial U_i}{\partial x_j}\right|} \quad (10)$$

The above invariant formulation of this length scale better resolve small scale turbulent structure. The eddy viscosity and the damping function D_2 are computed using

$$\nu_T = \tilde{\nu}_T D_2 \text{ with } \quad D_2 = 1 - e^{-(\tilde{\nu}_T / A_1 \kappa \nu)^2} \quad (11)$$

The coefficient A_1 is set equal to 13.0.

C. Document Modification

The Low Reynolds Number (LRN) SAS form of the transport equation for $\tilde{\nu}_T$ can be written in the SAS form as

$$\frac{D\tilde{\nu}_T}{Dt} = C_1 S \tilde{\nu}_T D_2 f_p - C_2 \frac{\tilde{\nu}_T^2}{L_{vK-SAS}^2} - C_4 \frac{\tilde{\nu}_T}{S}\left(\frac{\partial^2 U_i}{\partial x_j^2}\frac{\partial^2 U_i}{\partial x_j^2}\frac{\partial \tilde{\nu}_T}{\partial x_j}\frac{\partial \tilde{\nu}_T}{\partial x_j}\right)^{1/2} + \frac{\partial\left(\Gamma_\nu \partial \tilde{\nu}_T / \partial x_j\right)}{\partial x_j} + E_{diff/dest} \quad (12)$$

where

$$f_p = \begin{cases} \min(1, \max(r^n, e^{-\frac{\tilde{\nu}_T}{50}})) & \text{if } (1 - L_{vK-SAS}^2 / L^2) > 0 \\ 1 & \text{otherwise} \end{cases} \quad (13)$$

$$r = \left(\frac{\partial^2 U_i}{\partial x_j^2}\frac{\partial^2 U_i}{\partial x_j^2}\frac{\partial \tilde{\nu}_T}{\partial x_j}\frac{\partial \tilde{\nu}_T}{\partial x_j}\right)^{1/2} / (\kappa S)^2$$

and is the destruction to production ratio and $\Gamma_\nu = \nu + \frac{\tilde{\nu}_T}{\sigma_\nu}$. A condition should also be imposed on f_p, i.e., $f_p = 1$ *if* $r < 0.001$ when expecting the model to operate in homogeneous shear flows. The main difference between the SAS formulation of the present model and the URANS formulation reported earlier by Elkhoury [1] resides in the handling of the destruction terms The invariant of this length-scale that has been used by Elkhoury [1] was based on the

URANS formulation, calculated using strain rate gradients, i.e., $L_{vK-URANS}^2 = S^2 / (\partial S / \partial x_j)(\partial S / \partial x_j)$. While this invariant length-scale works well for large-scale structures, the present SAS formulation is better in resolving small-scale turbulent structures and is defined by

$$\frac{1}{L_{vK-SAS}^2} = \frac{\left|\frac{\partial^2 U_i}{\partial x_j^2}\frac{\partial^2 U_i}{\partial x_k^2}\right|}{S^2} \quad (14)$$

Similarly, the destruction term that involves scale invariant $C_4 \frac{\tilde{\nu}_T}{S}\left(\frac{\partial S}{\partial x_j}\frac{\partial S}{\partial x_j}\frac{\partial \tilde{\nu}_T}{\partial x_j}\frac{\partial \tilde{\nu}_T}{\partial x_j}\right)^{1/2}$ in the original model [1] is replaced by $C_4 \frac{\tilde{\nu}_T}{S}\left(\frac{\partial^2 U_i}{\partial x_j^2}\frac{\partial^2 U_i}{\partial x_j^2}\frac{\partial \tilde{\nu}_T}{\partial x_j}\frac{\partial \tilde{\nu}_T}{\partial x_j}\right)^{1/2}$ in the present SAS formulation. In order to avoid computational difficulties, the diffusion/ destruction term is limited to $20\times$ *production*, i.e.,

$$E_{diff/dest} = E_p \tanh\left(\frac{E_1}{E_p}\right) \quad (15)$$

where $E_p = 20 C_1 S \tilde{\nu}_T$ and

$$E_1 = 3C_3\left(1-\frac{L^2_{vK-SAS}}{L^2}\right)\tilde{\nu}_T\left(\frac{\partial\tilde{\nu}_T}{\partial x_j}\frac{\partial\tilde{\nu}_T}{\partial x_j}\right)^{1/2}\frac{1}{L_{vK-SAS}} \quad (16)$$

The length-scale, L, is given by $1/L^2 = \left(\partial^2 S/\partial x_j^2 / S\right)$ and is remarkably similar to the one obtained by Rotta [10], and Menter and Egorov [2] when neglecting convection and diffusion terms in the kL equation and eliminating the turbulence kinetic energy with the help of the transport equation for k. In almost all flows $E_p >> E_1$ and the original formulation is retained. Only in case the length-scale, L, in the denominator, goes to zero, the $E_{diff/dest}$ smoothly switches to E_p .

The eddy viscosity is computed from

$$\nu_T = \tilde{\nu}_T D_1 \quad (17)$$

The damping functions D_2, in the production term, and D_1 are

$$D_2 = \frac{\nu+\nu_T}{\nu+\tilde{\nu}_T},\ D_1 = 1-e^{-\left(\frac{\tilde{\nu}_T}{\nu A_1}\right)^2} \quad (18)$$

The One-Eq.-SAS model's constants are $A_1 = 18.0$, $n = 0.123$, $\sigma_v = 0.7$, $C_1 = 0.157$, $C_3 = 0.24/1.95$, $C_4 = 1.794$ and C_2 follows from the logarithmic law as $C_2 = \left(C_1/\kappa^2 + 1./\sigma_v - 3C_3 - C_4\right)$. The A_1 constant in the original model was set to 17.5, while it is slightly tweaked to better fit the logarithmic overlap given the present SAS formulation.

III. Numerical Approach

The computations throughout this work were performed using the commercial software Fluent 16.2. The one-equation SAS and Menter one-equation models were solved utilizing the User Defined Scalars (UDS) capabilities that are available in the software. All models were solved using either the implicit density based or pressure based coupled solver. In shock-boundary-layer interaction flow test cases, the implicit density based solver with Roe flux was used with convergence acceleration techniques. Flow gradients were handled using the Green-Gauss node based method. The pressure based solver was also utilized for the cylinder test case, in which the momentum equations were discretized using the second order bounded central difference scheme. This was necessary to minimize numerical dissipation so as to resolve flow structure in the wake region of the cylinder. The standard interpolation scheme was used in calculating the cell-face pressures. A second order time-accurate formulation was used in transient computations. In both solvers, convective terms were handled using second order upwind-based discretization scheme with under-relaxation factors of 0.8.

IV. Results

In all considered test cases, calculations were run fully turbulent. The present model was previously validated for the flow over a flatplate [1] and thus, this basic test case will not be repeated in the present work. In all test cases, a minimum convergence criterion of 1×10^{-3} of scaled residuals of all flow variables was obtained. Furthermore, all computations were performed on the IBM HPC nextScale M5 with 96 cores of Intel(R)-Xeon(R)-CPU-E5-2667-v3-@-3.20 GHz running with double precision at 4 Teraflops.

A. Transonic Flow Over NACA 0012 Airfoil

This is a challenging test case for turbulence models as it involves shock-induced separation. Thus, the sensitivity of the turbulence models is expected to be considerably more pronounced. In addition, prediction of the aft shock pressure recovery is also a major challenge, where many turbulence models fail to predict. The airfoil's angle of attack was set at 2.26° with a Mach number of 0.799. The Reynolds number, based on the chord and the freestream velocity, was 9.0×10^6. The computations were performed on a structured 257 × 65 grid with 34 points laying in the wake downstream the trailing edge of the airfoil. The far field was located approximately 16 chords from the airfoil surface with the first grid point in the off-body mesh was located at an average of $y^+ \approx 1$. Fig. 1 shows the variation of the surface pressure coefficient as computed by the three considered models along with the measurement given by Harris [11]. Menter $(k\text{-}\varepsilon)_{1E}$ based model predicted a shock location too far downstream, and is followed by the SA model which returns an excellent post shock pressure recovery. The One-Eq.-SAS model returns a marked improvement in terms of the shock location and post shock Cp distribution.

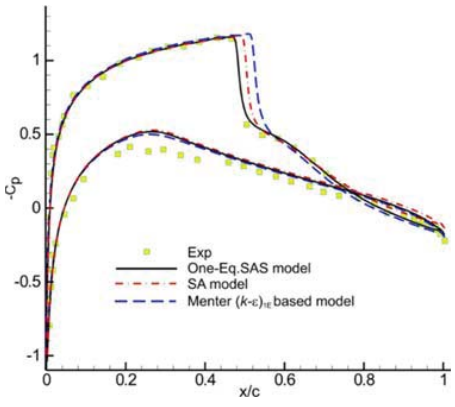

Fig. 1 Mean surface pressure distribution over the NACA 0012 airfoil

B. Transonic Flow Over Axisymmetric Bump

This test case is another shock-induced separation flow at a Mach number of 0.875 and a Reynolds number of 2.763×10^6 the experimental data are by Bachalo and Johnson [12]. The interaction of the shock-boundary-layer causes the flow to detach and reattaches further downstream on the cylinder. The computations were performed on an axisymmetric structured grid with 150 x 100 x 2 nodes with the first grid point located

at $y^+ \approx 0.82$. Mesh clustering was performed in the expected shock region. A sketch of the geometry showing the main flow features is depicted in Fig. 2. The surface pressure coefficient for the three considered models is shown in Fig. 3. Both the One-Eq.-SAS and Menter $(k\text{-}\varepsilon)_{1E}$ based models predict excellent shock location with acceptable pressure recovery distribution, whereas the SA model predicts a slightly delayed shock location. Figs. 4 and 5 present skin friction and streamwise velocity profiles, respectively. All three models capture the separation and reattachment points as indicated by the C_f profiles. Again, the One-Eq.-SAS and Menter $(k\text{-}\varepsilon)_{1E}$ based models predict overlapping velocity profiles upstream and downstream of the shock. The SA model predicts the best velocity profiles, which becomes evident downstream of the reattachment point. It is worth to note that the *k-ω-SST* model (not presented here) returned similar velocity profiles to those obtained by the One-Eq.-SAS and Menter $(k\text{-}\varepsilon)_{1E}$ based models.

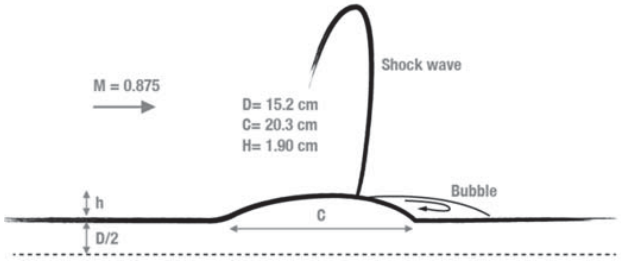

Fig. 2 Schematic of the bump showing the main flow features

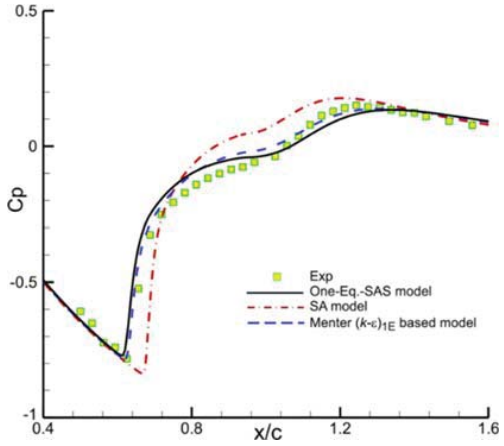

Fig. 3 Surface pressure coefficient for the transonic bump at M_∞=0.875 and *Re*=2.763 x 10^6

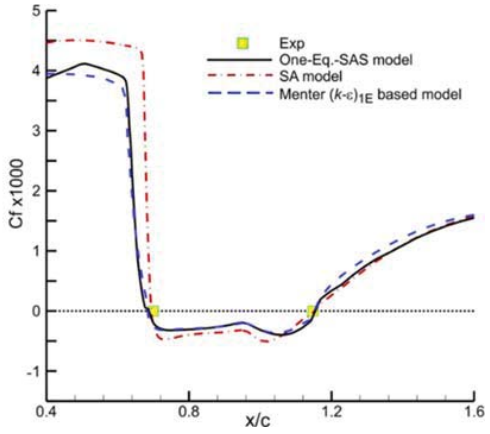

Fig. 4 Surface skin-friction distribution for the transonic bump at M_∞=0.875 and *Re*=2.763 x 10^6

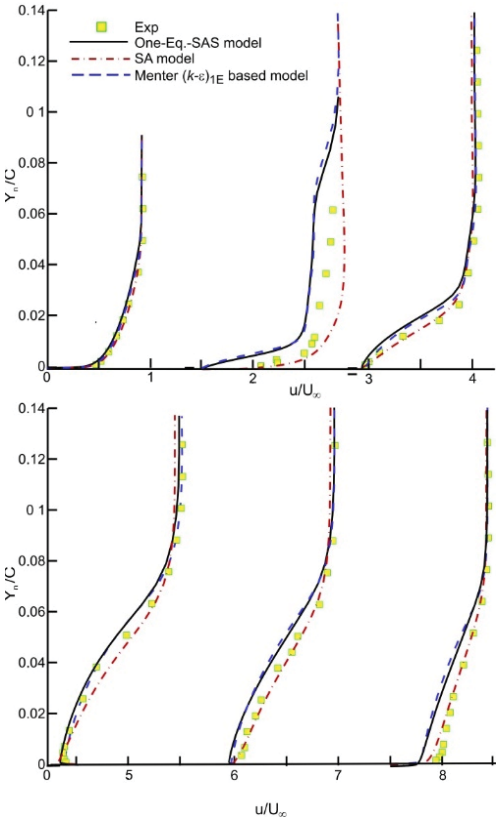

Fig. 5 Streamwise velocity profiles for the transonic bump at *x/c* =-0.25, 0.688, 0.813, 1.0, 1.125, and 1.375

C. Separated Flow Over the NACA 4412 Airfoil

The NACA 4412 is one of the most challenging test cases. It has been widely used in the literature to validate turbulence models due to flow separation associated with the relatively high angle-of-attack, which was set at 13.87°. The airfoil's Reynolds number was set at 1.52×10^6 based on the chord with a Mach number of 0.2. This angle-of-attack is high enough to induce adverse pressure gradient on the suction side of the airfoil that rapidly thickens the boundary layer, leading to flow

separation. The flow solver was used on a grid size of 257×91 with 191 nodes lying on the airfoil surface. An outer boundary extent of approximately 15 chords and the first off-body mesh had a minimum y^+ magnitude of ≈1. Fig. 6 presents a comparison of the mean velocity profiles at several locations along the suction side of the airfoil. The Experimental measurements are those by Coles and Wadcock [13]. Transition on the airfoil was accounted for by tripping the boundary layer on the upper and lower surfaces of the airfoil at x/c=0.023 and 0.1, respectively. The SA model predicts separation that falls within the experimental range [13] of x/c =0.7-0.8. This is followed by the One-Eq.-SAS model, which also predicts separation within that range at $x/c \approx 0.796$. A delayed separation is predicted by Menter's $(k\text{-}\varepsilon)_{1E}$ model, taking place at $x/c \approx$ 0.94. Furthermore, it was found that various LRN formulation had negligible effect on the prediction of the separation point [6], which was thought to be very much related to the HRN form of the transport equation for $\tilde{\nu}_T$.

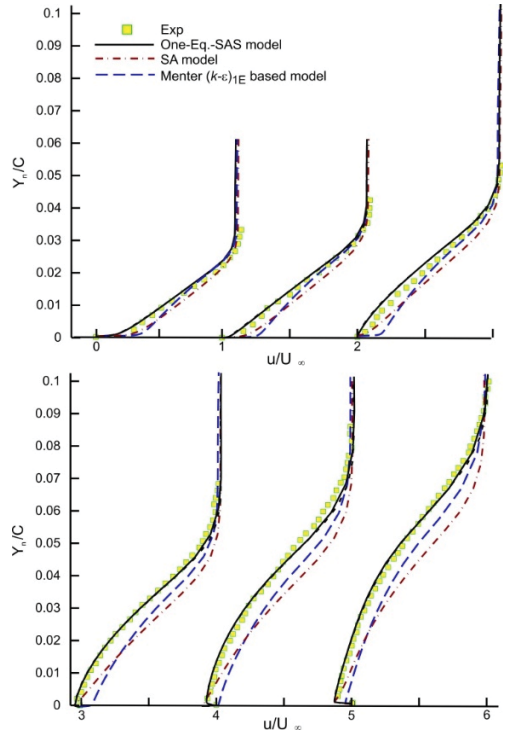

Fig. 6 Mean velocity profiles for the NACA 4412 airfoil at x/c=0.675, 0.731, 0.786, 0.842, 0.897, and 0.953 on the suction surface of airfoil

D.Transonic Flow Over the ONERA M6 Wing

This is a 3-D test case in which turbulence models are assessed against experimental findings to assess their capabilities of capturing the shock location at various wingspan location. Experimental data are given by Schmitt and Charpin [14]. The flow had a Mach number of 0.8395 with a Reynolds number set at 11.7 x 10^6 based on the aerodynamic mean chord of the wing, which had an angle-of-attack of 3.06° deg. The computations were performed on a grid size of 3.83 x10^6 nodes with 30 layers of surface inflation and a first layer height of 1x10^{-6} m, resulting in a $y^+ \approx 0.68$. Contours of surface pressure on the suction side of the wing for the considered three turbulence models are depicted in Fig. 7. The stagnation pressure region at the leading edge followed by a clear demarcation of high and low pressure contour on the suction side of the wing, indicating the presence of a shock wave. This shock which is termed as the "λ-shock" in literature can be clearly observed by the predictions of the SA and the One-Eq.-SAS models. However, a subtle variation in pressure contours is observed across the shock by Menter $(k\text{-}\varepsilon)_{1E}$ based model.

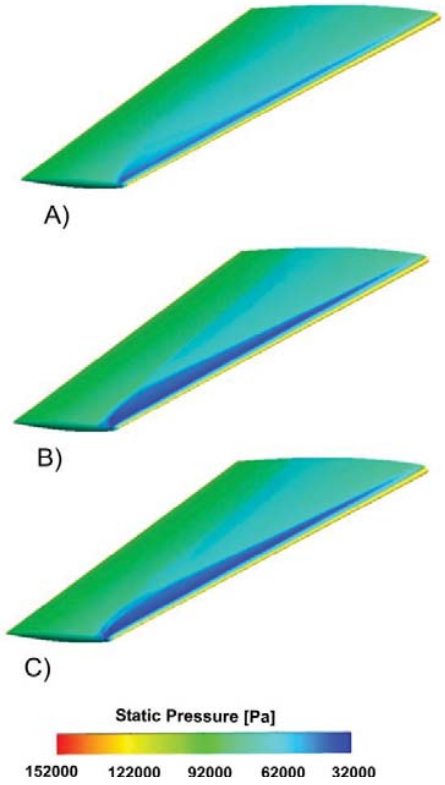

Fig. 7 Surface pressure contours over the ONERA M6 Wing at M_∞=0.8395, α=3.06°, and Re=11.7 x 10^6, (A) Menter $(k\text{-}\varepsilon)_{1E}$ based model, (B) SA model (C) One-Eq.-SAS model

Surface pressure coefficient vs x/c at several wing span locations is depicted by Fig. 8. The presence of the double shock wave on the suction side of the wing along the chordwise direction is clearly detected. The distance between the double shocks diminishes and they merge into a single shock wave as the wing tip is approached. Cp variation predicted by both the SA and the One-Eq.-SAS models are in accord with the experiments up to about 80% of the wing span. A slight discrepancy is noticed however, in the near vicinity of the shock wave towards the wing tip at 90 and 95% of the wing span. On the contrary, Menter $(k\text{-}\varepsilon)_{1E}$ based model fails to accurately predict Cp variation all over the wing span. Although the model predicts an adequate Cp variation at 20 % and 44 % of the wing span, it fails to replicate the Cp variation prior to the first shock

wave. This discrepancy in the results intensifies at further wing span stations towards the tip.

E. Flow Past a Circular Cylinder

This test case involves massive flow separation behind a circular cylinder, the inclusion of which was intended to demonstrate the capability of the One-Eq.-SAS and Menter (k-ε)$_{1E}$ based models to operate in a Scale-Resolved-Simulation mode. For all models, the bounded central differencing scheme was selected as it involves acceptable numerical dissipation that is small enough not to affect the evolution of small-scale turbulent structures. The set-up of this test case is based on the experimental work of Warschauer and Leene [15] with a Reynolds number of 1.2×10^6 based on the diameter of the cylinder. The spanwise extension of the domain was 4xD, which is considered acceptable for resolving turbulent flow structures. Periodic boundary condition was imposed in the spanwise direction while velocity inlet and pressure outlet boundary conditions were implemented at the inlet and the outlet of the domain. Boundaries in the transvers direction were treated with symmetry conditions. A grid with 6.38×10^3 nodes was initially implemented with a time step of 10^{-4}. Grid adaptation technique was employed after the elapse of 1000 time steps downstream the cylinder in the wake region. The final grid had 2.73×10^6 nodes, which was achieved after two successive adaptations. Time-averaged results are reported after the elapse of 10^5 time steps.

Instantaneous turbulent flow structures colored by eddy viscosity ratio downstream of the cylinder are shown in Fig. 9. It is apparent that both the Menter (k-ε)$_{1E}$ based and the One-Eq.-SAS and models resolve large and small scales in the vortex street downstream the cylinder, with a better capability of adapting to these scales is demonstrated by the latter model. The SA model however, exhibits a typical URANS simulation accompanied by high levels of eddy viscosity ratio, indicating a high level of dissipation. Fig. 10 shows a comparison of the time-averaged wall Cp distribution between the three models and available experimental data. Results of both the Menter (k-ε)$_{1E}$ based and the One-Eq.-SAS and models are similar with a discrepancy that was also reported by Menter et. al. [5] with SST-DES and was due to the differences between the experiments and the CFD set-up. The SA model however, predicts a remarkably similar pressure profile up to $\theta \approx 135^o$, which raise suspicion as to whether this discrepancy is due to the mismatch between the experiment and the CFD set-up or it is simply a failure of turbulence models.

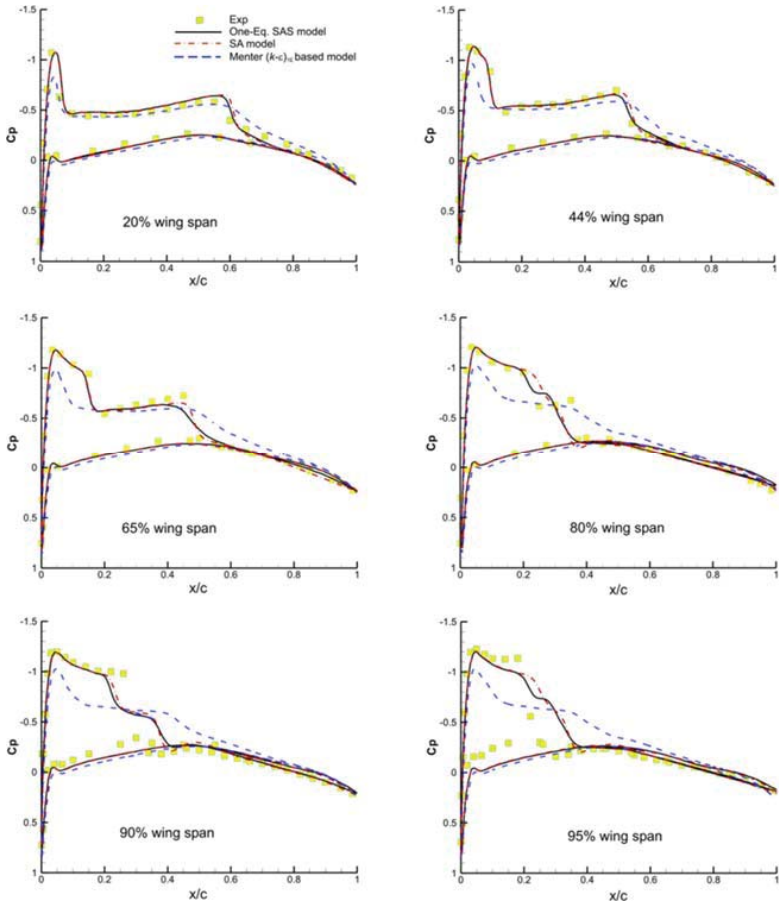

Fig. 8 Surface pressure coefficient at M_∞=0.8395, α=3.06^o, and Re=11.7 x 10^6 for the ONERA M6 Wing at different spanwise location

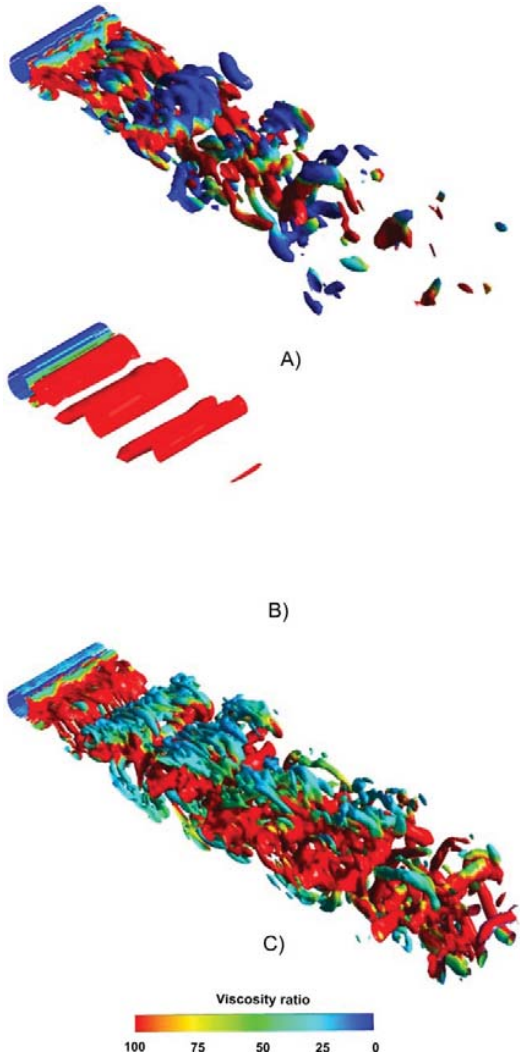

Fig. 9 Circular cylinder in a cross flow at Re=1.2 x10^6, (A) Menter $(k\text{-}\varepsilon)_{1E}$ based model, (B) SA model (C) One-Eq.-SAS model. Iso-surface of Q=S^2-Ω^2= 25, colored by the eddy viscosity ratio

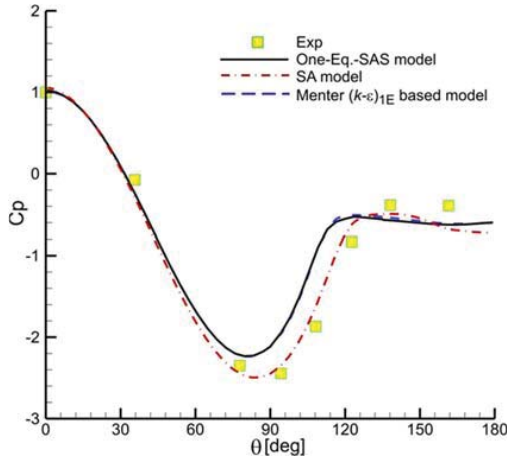

Fig. 10 Mean surface pressure coefficient for the circular cylinder at Re=1.2 x10^6

V. Conclusion

Three turbulence models that belong to the single-equation closure family have been examined over a wide range of test cases that included adverse pressure gradient, shock-boundary-layer interaction, and globally unstable flow with massive separation. The One-Eq.-SAS and Menter $(k\text{-}\varepsilon)_{1E}$ based models operate in SRS mode while the SA model operates in the RANS mode, which is due to the formulation of the destruction term that renders the models less dissipative. A key feature of the SAS models is that they produce turbulent flow structures similar to LES and DES without suffering from the explicit grid sensitivity and they do not require unsteady inflow condition. The latter is important in internal flow problems where a fully developed profile is imposed at the inlet.

The performance of Menter $(k\text{-}\varepsilon)_{1E}$ based model was worst in predicting shock-boundary-layer interaction flows in at least two out of the three considered cases. In addition, the model did not perform well in predicting velocity profiles in adverse pressure gradient flows. This in turn is attributed to the characteristics of its mother $k\text{-}\varepsilon$ turbulence closure. The SA model comes second in terms of predicting shock wave locations. It predicts the best velocity profiles for the transonic flow over the axisymmetric bump. For the NACA 4412 airfoil, the SA model predicts the separation point within experimental range however; velocity profiles are not in accord with the experiments. The One-Eq.-SAS model performs fairly better in all test cases except for the wall Cp distribution of the cylinder and velocity profiles for the transonic flow over the axisymmetric bump test cases.

Nomenclature

A_1 = turbulence-model closure coefficients
C_f = skin-friction coefficient
C_p = wall pressure coefficient
C_1, C_2, C_3, C_4, $C_{\varepsilon 1}$, $C_{\varepsilon 2}$ = turbulence-model closure coefficients
$D(\ )/Dt$ = material derivative
D_1, D_2 = turbulence-model wall-damping functions
E_{dest} = turbulence-model destruction term, m^2/s^2
$E_{diff/dest}$ = turbulence-model diffusion/destruction term, m^2/s^2
E_p = limiter based on turbulence production, m^2/s^2
f_p = turbulence-model production limiter
f_{v1}, f_{v2} = turbulence-model damping functions
k = turbulence kinetic energy m^2/s^2
$L_{VK\text{-}SAS}$ = von Kármán length-scale, m
L = mixing length scale, m
Re = Reynolds number
r = destruction-to-production ratio
S = strain-rate magnitude, s^{-1}
Ω = vorticity-rate magnitude, s^{-1}
ν = kinematic viscosity, m^2/s
y^+ = dimensionless, sublayer-scaled distance
ε = turbulence dissipation rate, m^2/s^3
κ = von Kármán constant
$\tilde{\nu}_T, \nu_T$ = kinematic eddy viscosity, m^2/s
σ_ν, σ = turbulent diffusion coefficient

Subscripts

i, j, k = Cartesian vector and tensor notation indices

∞ = freestream

T = turbulent

REFERENCES

[1] Elkhoury, M., "Partially Lagging One-Equation Turbulence Model", AIAA Journal, Vol.53, Issue 12 pp. 3661-3673. doi: 10.2514/1.J054018
[2] Menter, F. R., Egorov, Y., "A Scale-Adaptive Simulation Model Using Two-Equation Models", AIAA Paper-2005-1095. Reno NV. 2005.
[3] Menter, F. R., "Eddy Viscosity Transport Equations and Their Relation to the k-ε Model", Journal of Fluids Engineering, Vol. 119, 1997, pp. 876–884. doi:10.1115/1.2819511
[4] Bradshaw, P., Ferriss, D.H., and Atwell, N.P., "Calculation of boundary Layer Development Using the Turbulent Energy Equation", J. Fluid Mech., Vol. 23, 1967, pp31-64.
[5] Menter, F. R., Kuntz, M., and Bender, R., "Scale-Adaptive Simulation Model for Turbulent Flow Predictions", AIAA Paper-2003-0767. Reno NV. 2003.
[6] Elkhoury, M., "Modified Menter Model in Comparison with Recently Developed Single-Equation Turbulence Closures", AIAA Journal, Vol. 49, No. 7, 2011, pp. 1399–1408. doi: 10.2514/1.J050648
[7] Elkhoury, M., "A Low-Reynolds-Number One-Equation Model of Turbulence", The Aeronautical Journal, Vol. 112, No. 1128, 2008, pp. 101–108.
[8] Elkhoury, M., "Assessment and Modification of One-Equation Models of Turbulence for Wall-Bounded Flows", Journal of Fluids Engineering, Vol. 129, 2007, pp. 921–928. doi:10.1115/1.2743666
[9] Spalart, P., and Allmaras, S., "A One-Equation Turbulence Model for Aerodynamic Flows", AIAA 92-0439, 1992.
[10] Rotta J. C., Turbulente Strömumgen. BG Teubner Stuttgart, 1972.
[11] Harris, C., "Two-Dimensional Aerodynamic Characteristics of the NASA 0012 Airfoil in the Langley 8-Foot Transonic Pressure Tunnel", NASA TM-81927, 1981.
[12] Bachalo, W. D., and Johnson, D. A., "Transonic, Turbulent Boundary-Layer Separation Generated on an Axisymmetric Flow Model", AIAA Journal, Vol. 24, No. 3, 1986, pp. 437-443.
[13] Coles, D., and Wadcock, A. J., "Flying HotWire Study of Flow Past an NACA 4412 Airfoil at Maximum Lift", AIAA Journal, Vol. 17, 1979, pp. 321–328. doi:10.2514/3.61127
[14] Schmitt, V. and F. Charpin, "Pressure Distributions on the ONERA-M6-Wing at Transonic Mach Numbers", Experimental Data Base for Computer Program Assessment. Report of the Fluid Dynamics Panel Working Group 04, AGARD AR 138, May 1979.
[15] Warschauer, K. A. and Leene, J. A., "Experiments on mean and fluctuating pressures of circular cylinders at cross flow at very high Reynolds number", Proceedings of the international conference on wind effects on buildings and structures, Tokyo, pp.305-315, 1971.

M. Khoury is currently an associate professor of mechanical engineering at the Lebanese American University. His research interests fall primarily within the areas of renewable energy and fluid mechanics (especially wind turbines, wind power harvesting, and turbulence modeling). He has published in numerous internationally recognized journals such as the AIAA Journal, Energy Sources, ASME Journal of Fluids Engineering etc. He has been teaching courses and supervising final year projects in the area of solar/thermal energy since 2004.